Rock Mechanics and Rock Engineering (2024) 57:1117–1135
https://doi.org/10.1007/s00603-023-03613-8

ORIGINAL PAPER

Mechanical Properties and Damage Evolution Characteristics of Thermal Damage Basalt Under Triaxial Loading

Gang Wang[1,2,4] · Leibo Song[1,2] · Xiqi Liu[3] · Xiaoming Ma[4] · Jiaxing Qiao[1,2] · Hao Chen[1,2] · Longke Wu[5]

Received: 16 May 2023 / Accepted: 7 October 2023 / Published online: 1 November 2023

Abstract

To explore the mechanical properties and damage characteristics of basalt under high temperature and high pressure, triaxial compression tests are conducted on thermal damage rock samples, and the evolution process from progressive damage to macroscopic failure of rock is tracked and quantified by CT image reconstruction and acoustic emission technology. The results show that: (1) the ability of basalt to resist load and deformation changes from slight enhancement to rapid deterioration with the increase of temperature, and 600 ℃ is its threshold. The failure mode of rock gradually changes from brittleness to plasticity with the increase of temperature, and its post-peak stress gradually presents certain plastic flow characteristics. (2) With the increase of temperature, the initial damage variable D_0 of basalt presents a stage feature of changing from low-speed development to rapid growth. When the temperature exceeds 400 ℃, the total damage variable D will have obvious precursor characteristic of small increase before the drastic change, and this characteristic will become more obvious with the increase of temperature. (3) The main mineral types of basalt hardly change with the increasing temperature, while the temperature has a certain influence on the proportion of some components. The proportion of anorthite and enstatite shows the changing trend of first decreasing and then increasing, while the evolution of andesine is opposite, and the proportion of other mineral components is basically unchanged. (4) The main reason for the improvement of mechanical properties of basalt within the temperature threshold is that the expansion of mineral particles and the constraint of confining pressure promote the closure of internal primary cracks and increase the compactness. However, when the heat treatment temperature of basalt exceeds the threshold value, the structural deterioration caused by heat treatment is gradually prominent, and the defects generated play a leading role in the mechanical properties of rock.

Highlights

- The mechanical properties of thermal damage basalt under triaxial loading were clarified and its temperature threshold was obtained
- The evolution process from progressive damage to macroscopic failure of basalt was tracked and quantified
- The microscopic failure mechanism of thermal damage basalt was revealed
- The number of tensile cracks of saturated coal increased with the cyclic loading frequency due to the prominent lag effect of strain behind stress.

Keywords Rock mechanics · High temperature effect · Basalt · Mechanical behavior · Damage characteristics

✉ Leibo Song
song_leibo@163.com

[1] School of Civil Engineering, Shaoxing University, Shaoxing 312000, Zhejiang, China

[2] Collaborative Innovation Center for Prevention and Control of Mountain Geological Hazards of Zhejiang Province, Shaoxing University, Shaoxing 312000, Zhejiang, China

[3] Hydraulic Engineering Research Calculation, Pearl River Water Resources Research Institute, Guangzhou 510611, Guangdong, China

[4] Huahui Engineering Design Group Co., Ltd, Shaoxing 312000, Zhejiang, China

[5] Guangxi Conmmunication Design Group Co., Ltd, Nanning 530029, Guangxi, China

1 Introduction

The increasing demands for energy, resources and underground space promote mining and geothermal development and other projects to develop in the deep at an unprecedented speed (DasGupta et al. 2022; Pan et al. 2021; Song et al. 2022; Wang et al. 2023a, b; Niu et al. 2023). At present, the depth of mining development reaches 1500 m, the depth of geothermal resources exploitation exceeds 3000 m, and the depth of oil field exploitation reaches 7500 m. The deep engineering construction tends to be normalcy (Li et al. 2021). The deep rock mass engineering is located in complex geological environment such as high temperature and high ground stress. It will lead to various changes in rock mass structure, composition and macro-mechanical properties, seriously threatening the construction safety and service life of the project (Miao et al. 2021; Braun et al. 2021). Therefore, it is of great scientific value and engineering guiding significance to study the physical and mechanical properties and damage characteristics of deep rock mass under high temperature and high ground stress.

Currently, a lot of research has been conducted on the physical properties and static mechanical characteristics of rocks under high temperature and high pressure, and abundant theoretical and application results have been obtained. Yin et al. (2021) took coarse-grained and fine-grained granite as the research object, and found that the thermal expansion coefficient of granite increased linearly with the temperature increasing from 100 to 400 ℃, and the thermal expansion coefficient of coarse-grained granite was 1.52 times that of fine-grained granite on average. Gautam et al. (2018) found that the threshold temperature of the thermophysical properties of Jalore granite is 300 ℃. When the temperature exceeded 300 ℃, the deterioration of granite samples was aggravated, leading to a significant decrease in its thermal conductivity and longitudinal wave velocity. Liu et al. (2021) and Shi et al. (2020) studied the strength and deformation characteristics of sandstone under high temperature and high pressure. The results showed that the mechanical properties such as compressive strength and elastic modulus of rocks presented a changing trend of first increasing and then decreasing with the increase of temperature. Su et al. (2017) conducted triaxial tests on veined marble samples under different temperatures, and the results showed that high temperature had a significant weakening effect on the triaxial compressive strength, elastic modulus and secant modulus of marble, and significantly affected the mechanical behavior. Ma et al. (2019) simulated the coupled environment of temperature and stress field of rocks in deep strata, indicating that high temperature of 400 ℃ can enhance the strength and elastic modulus of granite. The above research systematically analyzes the macroscopic physical and mechanical properties of deep rock under high temperature environment. However, the difference of macro-mechanical properties of rocks is actually caused by structural or compositional changes such as meso-defects (Sangsefidi et al. 2021; Liu et al. 2023). Liu et al. (2022) found that the internal composition and structure of skarn changed under high temperature based on SEM (scanning electron microscopy) and XRD (X-ray diffraction) analysis technology, which was the main reason for the change of rock mechanical properties. Shi et al. (2020) thought that the change of mineral composition and defects of high temperature marble is an important reason for the change of its dynamic mechanical properties. Therefore, it is of great significance to study the quantitative description of microstructure characteristics, the rock damage and the mineral composition characteristics. In addition, with the rapid development of deep large-scale rock mass engineering, the types of high temperature surrounding rocks have also expanded from granite, marble and sandstone to other categories. The research on thermal damage mechanical properties of other rocks also needs to be promoted urgently.

Basalt is an important part of the earth's oceanic crust and continental crust. It has many characteristics such as high compressive strength and wide distribution, and is a common rock type in rock mass engineering (Garcia-Ramonda et al. 2022; Silva et al. 2021; Wang et al. 2021a, b). In this study, basalt is taken as the research object. Through the reconstruction of CT (Computerized Tomography) image of thermal damage basalt, the spatial distribution characteristics of porosity and cracks in basalt after high temperature treatment are analyzed at the microscopic level. Based on triaxial loading test and acoustic emission monitoring, the evolution process from progressive damage to macroscopic failure of rock is obtained. The research results are of great significance for understanding the thermal damage evolution of basalt under high temperature environment in the deep, reasonably selecting engineering structural parameters and scientifically evaluating the stability of rock mass.

2 Experimental Procedure

2.1 Sample Preparation and Test Equipment

Basalt samples are taken from Pingjiang County, Hunan Province, China. At normal temperature, the rocks are lead gray, dense and hard, and the texture is uniform. The composition analysis and microscopic detection of basalt at normal temperature are carried out by the X-ray diffraction device and the SEM. As shown in Fig. 1(a), through the

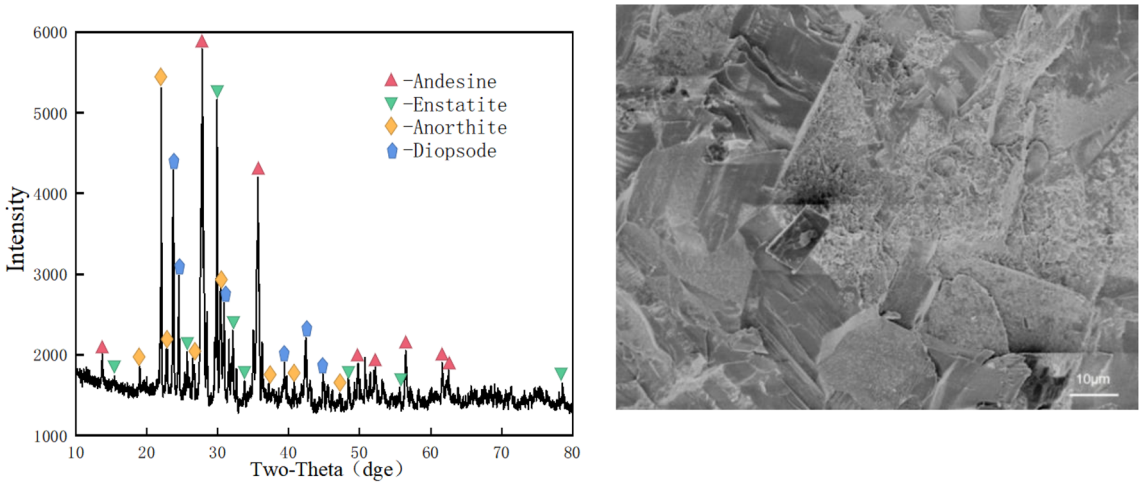

(a) XRD analysis (b) SEM images

Fig. 1 Composition and microstructure of basalt at room temperature

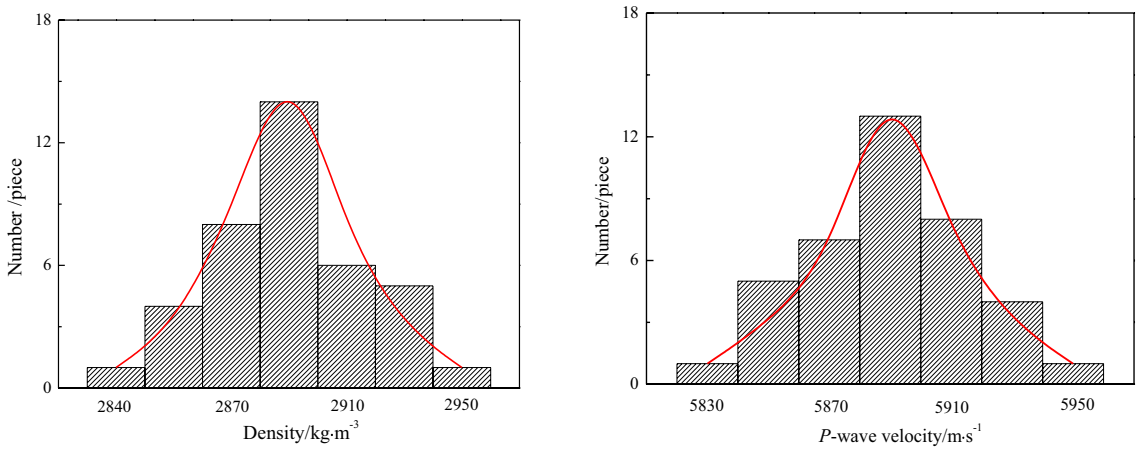

(a) Density distribution (b) Distribution of longitudinal wave velocity

Fig. 2 Statistics of density and wave velocity of basalt samples

phase analysis of the material, it is found that the mineral components mainly include andesine and enstatite, and the secondary minerals include anorthite and diopside. As can be seen from Fig. 1(b), basalt has a high degree of recrystallization, uniform and compact grain arrangement, and a massive structure as a whole. The interior of the rock is intact and compact, without any other obvious crack defects.

The selection of test samples meets the requirements of the same area, the same batch and similar mechanical properties. According to the International Society for Rock Mechanics (ISRM) standards (Brown 1981), cylindrical standard samples with a diameter of 50 mm and a height of 100 mm are prepared. The processed samples are initially screened, and samples with obvious natural or processing defects are eliminated. Then, the dimensions and longitudinal wave velocity of the samples are measured, and abnormal basalt samples are excluded. The parallelism and flatness of two end faces of sample are within 0.02 mm. The longitudinal wave velocity of basalt samples is between 5835 and 5947 m/s, and the density is between 2.842 and 2.922 g/mm^3 (Fig. 2). The dispersion is small and the distribution characteristics basically obey the normal distribution law, which can ensure the reliability of subsequent tests.

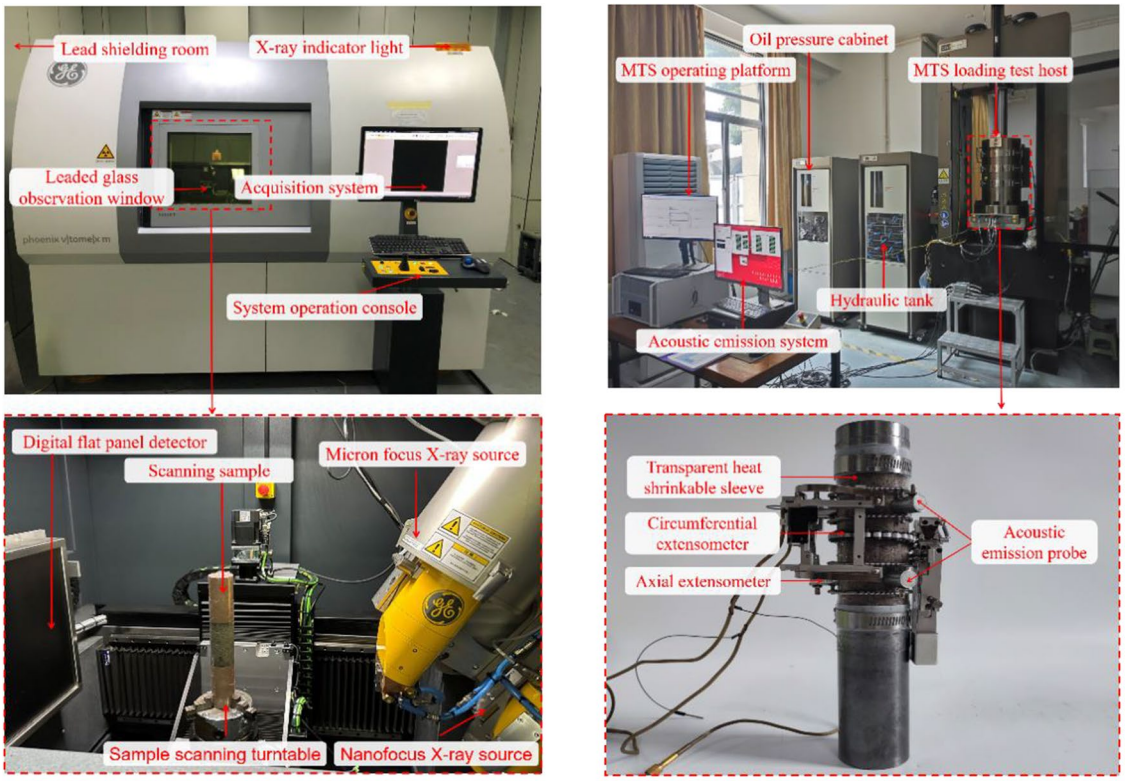

(a) Phoenix v|tome|x m CT system (b) MTS 815 rock mechanics test system

Fig. 3 Test system

The basalt samples after heat treatment are scanned by the Phoenix v|tome|x m micro-focus CT scanning system shown in Fig. 3(a). The system consists of micron and nanometer ray tubes, a carrier rotating table and X-ray detector. During the scanning process, a conical X-ray beam is generated by bombarding a tungsten metal target with high-energy electrons and focusing on the 3608 rotating carrier table. Through the detection panel, the full-range ray pictures of the rock sample on the carrier table can be automatically captured, which can realize the three-dimensional measurement and nondestructive analysis of the internal structure of the rock (Kuncham et al. 2022). The MTS815 rock mechanics test system shown in Fig. 3(b) is used for triaxial compression test (Wang et al. 2021a, b). The system is composed of test unit, loading unit and control unit. It is equipped with a servo controlled full-automatic pressurization and measurement system. The loading is stable and the test is accurate. Its maximum vertical load is 4600 kN, and the overall stiffness of the test frame can reach 11.0×10^9 N/m. During the loading process, the deformation of the sample is measured by high-precision axial extensometer and circumferential extensometer, respectively.

2.2 Test Design

The basalt samples are heat treated, and the rock samples are divided into 6 groups (A ~ F) for 24 h of drying, with each group conducting three parallel tests. Using the KSL-1200X muffle furnace, the B-F group rock samples are subjected to high-temperature treatment at 200 ℃, 400 ℃, 600 ℃, 800 ℃, and 1000 ℃ (basalt melting at 1200 ℃). The heating rate is 20℃/min, and the power supply is cut off after maintaining the corresponding temperature for 1 h. The samples are placed in a furnace and cooled to room temperature. The heat treatment path is shown in Fig. 4(a). Rock samples before and after heat treatment are shown in Fig. 4(b). After high temperature treatment, the color of samples changes obviously. After heat treatment at 200℃, 400℃, 600℃, 800℃ and 1000℃, the lead gray color of rock samples at room temperature changes to brown cyan, flaxen, dark khaki, dark brown and purple black, respectively. It is mainly caused by the change of mineral composition in rocks under different temperatures.

The basic physical properties of the basalt are measured, and then the composition of the sample is tested. Furthermore, the internal structure of the sample is reconstructed

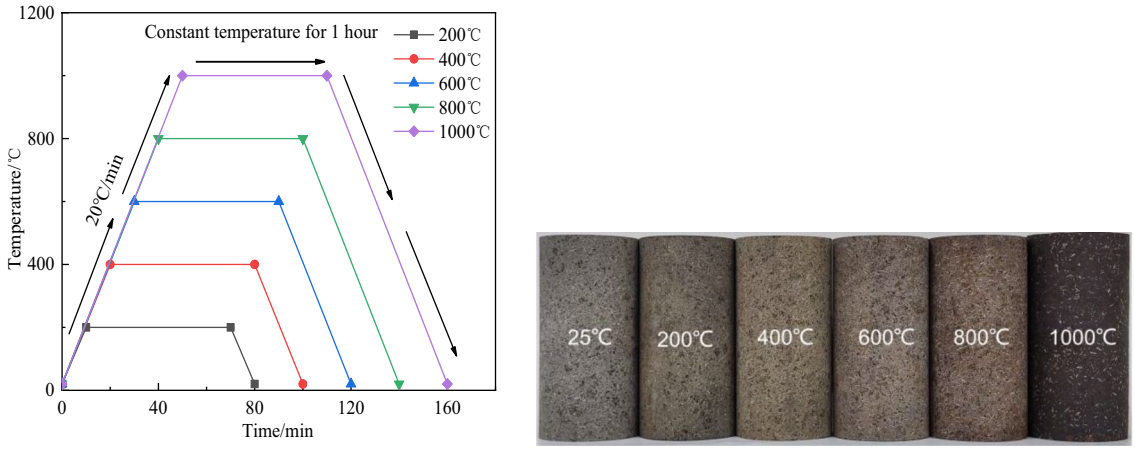

(a) Heat treatment path (b) Rock samples after heat treatment

Fig. 4 Heat treatment path and morphology of basalt after heat treatment

Fig. 5 Test process

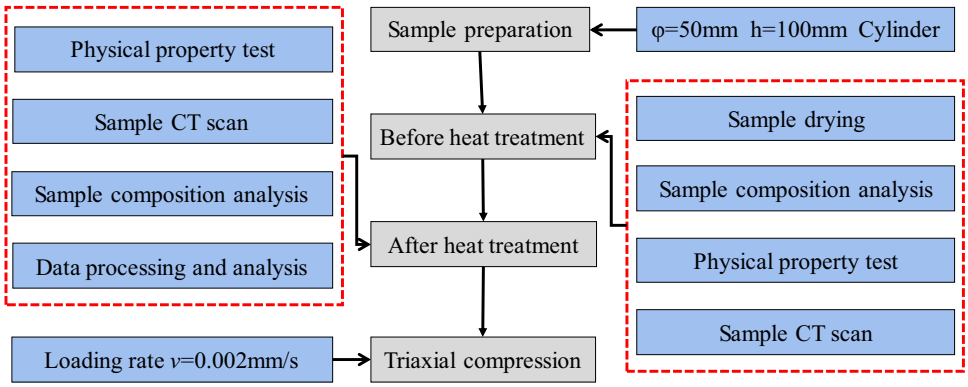

in three dimensions using the Phoenix v | tom | x m CT system, and the above steps are repeated after heating. Triaxial compression test is carried out based on MTS815 rock mechanics test system to obtain the mechanical properties of basalt after thermal damage and record the acoustic emission data during the failure process. Three repeatability tests were conducted under each condition. The specific test process is shown in Fig. 5.

In the process of CT scanning, current and voltage determine the number and penetration intensity of X-ray respectively. Due to the change of internal composition and structure of the sample after high temperature treatment, the penetration current and voltage need to be adjusted accordingly. In the pre-experiment, the voltage and current most suitable for the temperature are debugged to scan the sample. Each scanning time is 35 min, and the spatial resolution is within 40 μm. The axial load is applied at a loading speed of 0.002 mm/s using "displacement" control until the basalt sample fails. The whole loading process is monitored by PCI-II acoustic emission system, in which the threshold value is set to 40 dB and the sampling frequency is 1 MHz. Simultaneously, the axial and circumferential deformation of the sample is measured in real time by high-precision extensometer. The specific test scheme is shown in Table 1.

3 Results

3.1 Stress–Strain Curve

The typical triaxial stress–strain curve of basalt sample after high temperature treatment is shown in Fig. 6(a). The stress–strain curves of basalt are basically the same under different temperature heat treatments, and they all go through the stages of pore-fracture compaction, linear elasticity, unstable fracture development and post-peak failure as shown in Fig. 6(b). However, due to the different treatment temperatures, basalt shows certain differences under different high temperature treatments. The details are as follows:

Pore-fracture compaction stage (I): The basalt specimen has no significant crack defects, so the correspond-

Table 1 Experimental Scheme

Number	Heating rate ℃/min	Target temperature /℃	Cooling methods	Voltage /Kv	Current /uA	Confining pressure /MPa	Axial compression loading rate mm/s
A	20	25	Natural cooling	140 kV	150uA	30	0.002
B		200		140 kV	150uA		
C		400		140 kV	150uA		
D		600		140 kV	150uA		
E		800		130 kV	140uA		
F		1000		92 kV	190uA		

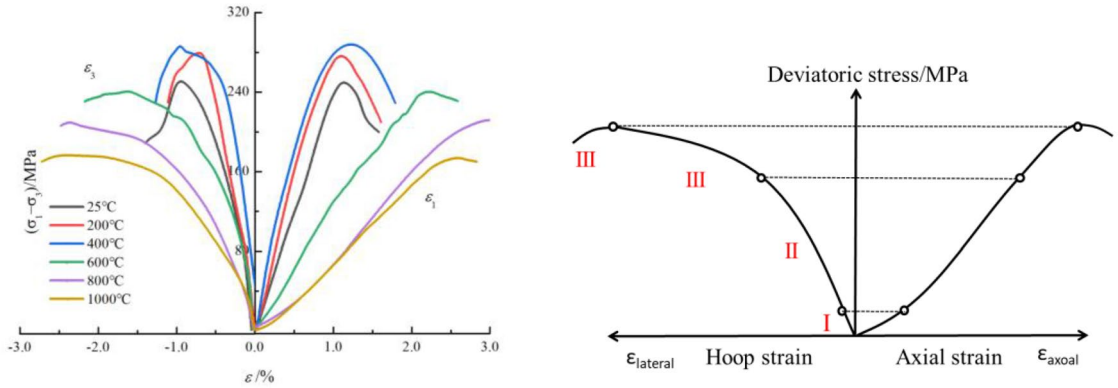

(a) Stress-strain curves of triaxial compression under different temperatures

(b) Typical triaxial compression stress-strain relationship

Fig. 6 Stress–strain curves of triaxial compression

ing pore and crack compaction characteristics of basalt sample at room temperature (25℃) are not obvious. The compaction stage of basalt after heat treatment at 200℃ and 400℃ is less different from that at room temperature. However, when the heat treatment temperature exceeds 400℃, the stress–strain curve of basalt shows obvious upward concave growth characteristics at the initial stage, i.e., high temperature promotes the rapid growth of defect volume in basalt samples. It takes more time to complete the closing process of internal pores and cracks under the combined action of axial pressure and confining pressure.

Linear elastic stage (II): The stress–strain curve of basalt shows linear growth characteristics under different heat treatments, due to its relatively dense internal structure. The rock enters the stage of elastic deformation. When the heating temperature is 400 ℃, the stress–strain curve slope is the largest, showing a strong ability to resist elastic deformation, and the elastic modulus reaches 159.2 9 GPa, which is 9.37% higher than that at room temperature. When the heating temperature exceeds 600℃, the slope of stress–strain curve decreases significantly, i.e., the ability to resist elastic deformation is obviously weakened. At 1000 ℃, the elastic modulus is only 67.40 GPa. Compared with the normal temperature state, the elastic modulus degradation of rock samples is as high as 53.72%.

Unstable fracture development stage (III): With the continuous increase of load, the stress–strain curve changes from linear growth to upward convex growth, showing obvious nonlinear characteristics. Under the drive of load, microcracks inside the rock constantly initiate and propagate, and the sample changes from elasticity to plasticity until the rock sample reaches the peak point of bearing limit. When the temperature exceeds 400 ℃, the pre-peak plastic characteristics of basalt samples tend to be obvious, and a certain yield platform appears.

Post-peak failure stage (IV): After the basalt reaches the bearing capacity, its internal structure is destroyed, and its bearing capacity is lost due to crack penetration. When the heating temperature is less than 400℃, the stress of basalt samples drops instantaneously after reaching the peak, showing strong brittleness character-

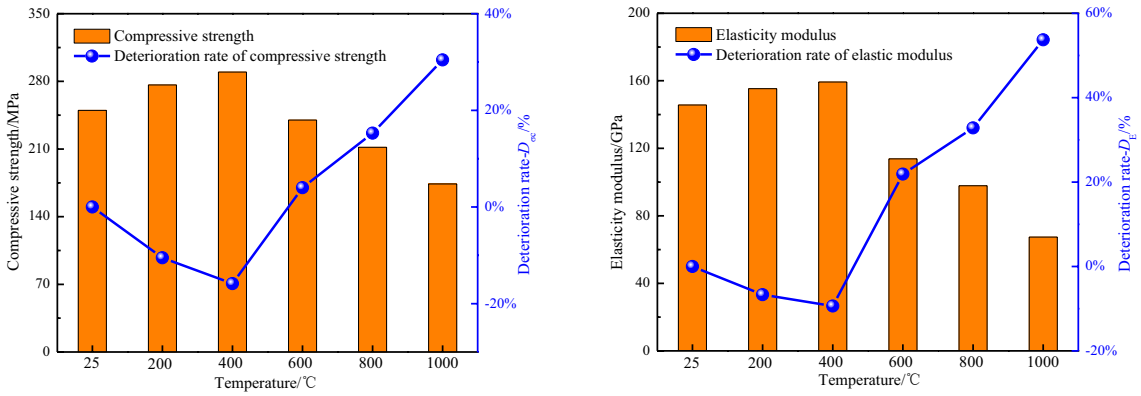

(a) Compressive strength (b) Elastic modulus

Fig. 7 Strength and deformation characteristics of basalt at different temperatures

istics. With the increase of heat treatment temperature, the instability of rock samples turns into a gradual process, and its post-peak stress gradually decreases and eventually fails, showing a certain plastic flow.

3.2 Strength and Deformation Characteristics

The strength and deformation characteristics of rock are crucial for the stability evaluation of rock mass (Huang et al. 2020; Song et al. 2023). The average compressive strength σ_c and elastic modulus E of basalt after different high temperature treatments are summarized in Fig. 7. To analyze the influence of temperature on strength and deformation characteristics, the parameter deterioration coefficient D_p is defined as Formula (1) with reference to the index at 25℃:

$$D_p = \frac{p_0 - p_i}{p_0} \times 100\% \tag{1}$$

where D_p is the parameter deterioration rate of basalt, p_0 is the parameter value of basalt at room temperature and p_i is the parameter value of basalt at a certain temperature. The parameter deterioration rates $D_{\sigma c}$ and D_E of triaxial compressive strength σ_c and elastic modulus E of basalt after different high temperature treatments are calculated respectively, and the results are shown in Fig. 7.

High temperature treatment affects the strength and deformation characteristics of basalt. With the increase of temperature, the compressive strength σ_c and elastic modulus E show a changing rule of increasing first and then decreasing, and the synchronous deterioration rates $D_{\sigma c}$ and D_E show a U-shaped evolution characteristic of first decreasing and then increasing, which is consistent with the phenomenon studied by many scholars such as Xu et al. (2015) and Liu and Xu (2015).

As shown in Fig. 7(a), when the heat treatment temperature is less than 400℃, the strength of basalt shows a phenomenon of stress strengthening with the increase of temperature. Compared with the compressive strength 250 MPa of basalt at 25℃, the compressive strength σ_c after heat treatment at 200 ℃ and 400 ℃ increases by 10.50% and 15.85%, respectively. The main reason is that the expansion of mineral particles causes the gradual closure of primary fractures, which increases the compactness of rocks and thus improves the mechanical properties to some extent. When the heat treatment temperature is higher than 600 ℃, the compressive strength σ_c decreases greatly. Compared with the 25 ℃, the compressive strength σ_c after heat treatment at 800 ℃ and 1000 ℃ decreases by 38.22 MPa and 79.11 MPa, respectively, and the deterioration rates $D_{\sigma c}$ reach 15.28% and 30.44%. At this stage, a large number of pores and cracks generated by thermal damage inside the sample play a dominant role.

The evolution of elastic modulus E with heat treatment temperature is similar to that of compressive strength (Fig. 7b). The average elastic modulus E of basalt at 25 ℃ is 145.63 GPa, showing a strong ability to resist deformation. When the heat treatment temperature is less than 400 ℃, the change amplitude of basalt stiffness with temperature is relatively small, showing a slight upward trend. Compared with 25 ℃, the elastic modulus E after heat treatment at 200 and 400℃ increases by 6.67% and 9.37%, respectively. When the heat treatment temperature is higher than 600℃, the elastic modulus E shows obvious deterioration. Compared with 25 ℃, the ability of rocks to resist deformation after heat treatment at 800 ℃ and 1000 ℃ is significantly reduced, and the elastic modulus E decreases by 47.812 GPa and 78.23 GPa, respectively, and the deterioration rates D_E are 32.83% and 53.72%.

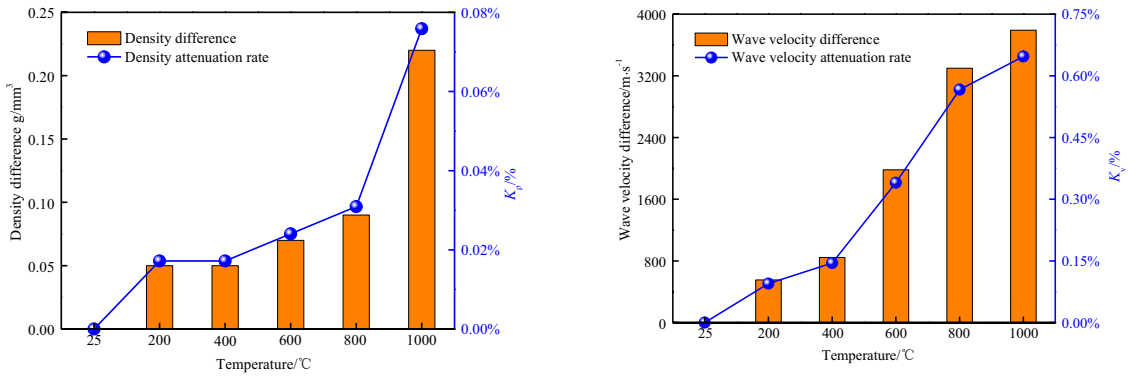

(a) Density difference and the attenuation rate

(b) Wave velocity difference and the attenuation rate

Fig. 8 Attenuation rate of physical parameters of basalt after different high temperature heat treatments

4 Discussion

4.1 Initial Damage of Heat Treatment Basalt

4.1.1 CT Testing Analysis

After high temperature treatment, the physical properties of basalt samples will change to some extent. The difference of rock densities and wave velocities under different working conditions is calculated, and the density attenuation rate K_ρ and longitudinal wave velocity attenuation rate K_v are defined, as shown in Formulas (2) and (3). As can be seen from Fig. 8, the difference of the densities and the wave velocities of basalt shows an increasing trend with the increase of heat treatment temperature. Compared with the physical and mechanical properties of basalt samples after high temperature treatment, it can be found that the evolution of density attenuation rate K_ρ and wave velocity attenuation rate K_v of basalt is similar. When the heat treatment temperature is less than 400 ℃, K_ρ and K_v increase at a low speed, and the high temperature treatment has little effect on the density and wave velocity. When the heat treatment temperature is greater than 400 ℃, K_ρ and K_v begin to increase sharply, indicating that large pores and cracks appear inside the sample, which leads to significant changes in density and wave velocity. When the temperature is 1000 ℃, the visible local cracks appear on the surface of the sample, and the changes of K_ρ and K_v of the rock sample are the most obvious at this temperature.

$$K_\rho = \frac{\rho - \rho_0}{\rho} \times 100\% \tag{2}$$

$$K_V = \frac{V - V_0}{V} \times 100\% \tag{3}$$

where, ρandρ_0, respectively, represent the density of the sample before and after heat treatment, and $v$andv_0, respectively, represent the wave velocity of the sample before and after heat treatment.

To clarify the initial damage of basalt better, CT technology is used for detection. Based on the principle of scanning imaging and the function of visual reconstruction, the results of CT tomography slices are imported into Avizo software for 3D image reconstruction to obtain 3D solid images and 3D fracture rendering images. As shown in Fig. 9, with the increase of heat treatment temperature, the microcracks of basalt gradually develop from the surface layer to its interior, and the number and size of the microcracks increase continuously and the microcracks gradually overlap to generate macrocracks. Specifically, compared with 25 ℃, microcracks of basalt below 400℃ are mainly distributed on the surface of the sample, the scale of the pores is generally small, and the pore volume is generally within 0.03 ~ 0.3mm^3, so the development of internal defects in the sample is not obvious. After high temperature treatment at 600 ℃, the number of pores on the basalt surface begins to increase, and the pore volume gradually increases. The number of microcracks and internal defects of basalt after heat treatment at 800 °C are further developed and develop to the center of the sample, forming a network structure of microcracks in different directions and levels, and the internal pore volume changes greatly. After heat treatment at 1000 °C, the internal microcracks of basalt converge and nucleate, and the surrounding pore structures are interconnected to generate crack groups, resulting in macroscopic staggered cracks. The propagation direction of the surrounding macrocracks is approximately parallel to the free surface, with a random distribution characteristic around the center of the specimen. The maximum

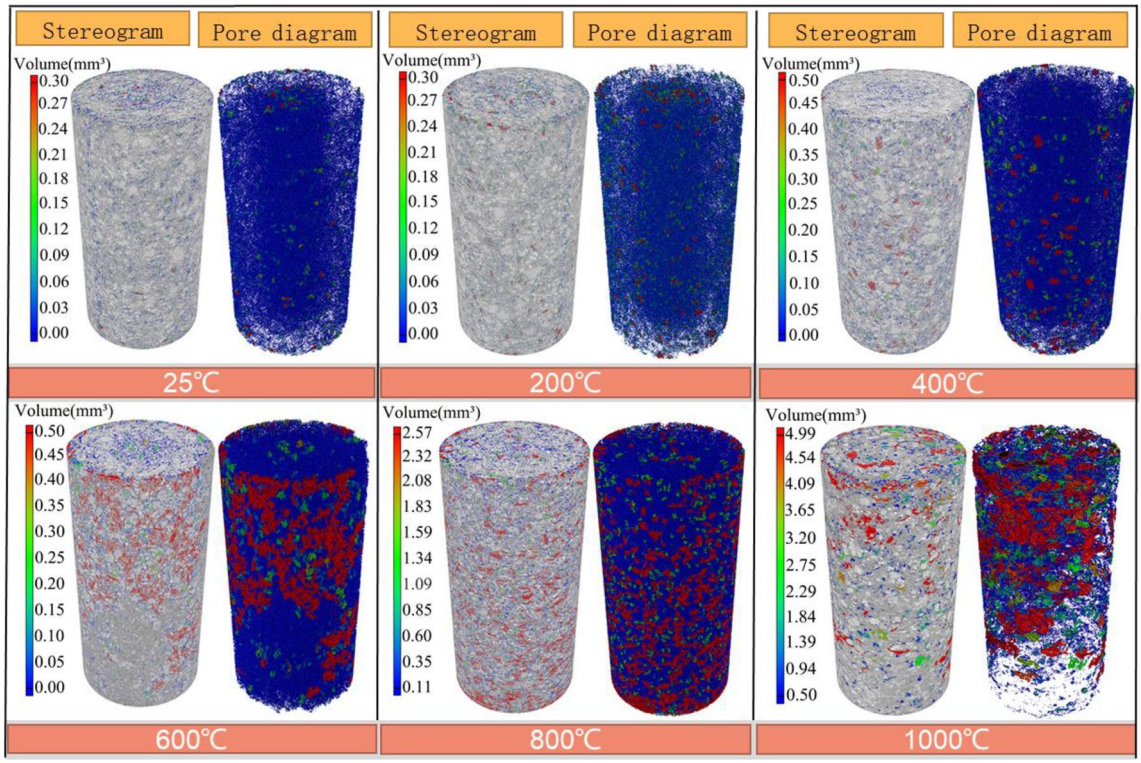

Fig. 9 Contrast of CT gray scale of basalt section before and after heating

pore volume has reached 4.99mm^3, and the deterioration of the internal structure of the rock sample is significant.

To further analyze the evolution of the number and scale of cracks, the porosity and pore volume range at different heat treatment temperatures are counted and plotted in Fig. 10. It can be found that when the heat treatment temperature is less than 600 ℃, the pore volume range and porosity of basalt show an upward trend, but the trend is relatively gentle. Compared with 25 ℃, the lower limit of the pore volume hardly changes, and the upper limit changes slightly, with the porosity from 6.86 to 7.56%. It indicates that although there is damage inside basalt in this temperature range, the scope and scale of the damage are small. When the heat treatment range is greater than 600 ℃, the lower limit of pore volume range changes less, the upper limit increases, resulting in a significant increase in porosity. After heat treatment at 800 ℃, the maximum pore volume of basalt reaches 2.75mm^3, and the porosity reaches 12.75%. At this moment, the internal structure of the basalt deteriorates significantly. After heat treatment at 1000 ℃, the pore volume range of basalt reaches 0.5 ~ 4.99mm^3, and the porosity is as high as 18.02%, resulting in a large range of structural damage inside the rock.

4.1.2 Initial Damage Variable

High temperature treatment will cause thermal damage to rocks, leading to the initiation and propagation of internal microcracks and directly affecting the mechanical properties of rocks (Gautam et al. 2018; Shi et al. 2020). To further quantify the thermal damage characteristics caused by high temperature, the initial damage variables of rocks are analyzed by CT calculation method (Ghamgosar et al. 2021; Vaneghi et al. 2021). Assuming that the cross-sectional area of the rock sample is A_u, its effective bearing area is A in the non-destructive state. When the sample has a certain level of damage, the effective bearing area of the rock sample is reduced to A_{cf}, then the damage variable is:

$$D_0 = \frac{A - A_{cf}}{A} = 1 - \frac{A_{cf}}{A} \tag{4}$$

If the density of non-destructive matrix rock is ρ_0 and the number of holes (cracks) in the resolution unit is n, the average density ρ in the resolution unit is:

$$\rho = \rho_0 \left(1 - \mathrm{n} \cdot \frac{A_0}{A}\right) \tag{5}$$

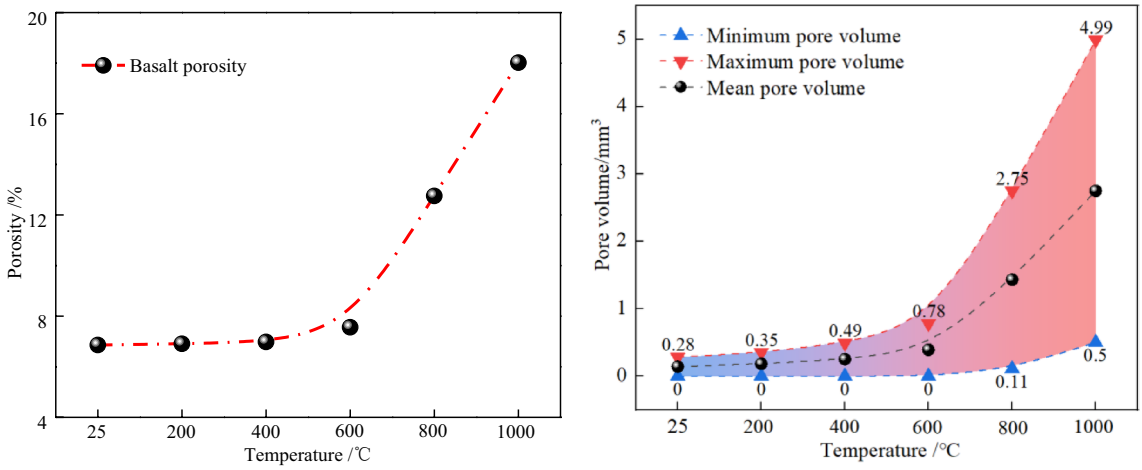

(a) Porosity changes at different temperatures

(b) Pore volume changes at different temperatures

Fig. 10 Variation law of porosity and pore volume at different temperatures

Table 2 Initial damage of rock samples at different temperatures

Temperature/℃	25	200	400	600	800	1000
Average initial damage *D*0	0.016	0.019	0.020	0.023	0.051	0.071
Damage growth ratio *k*	/	1.188	1.250	1.437	3.187	4.437

When the damage hole density isλ, the distribution law of n for different resolution units is:

$$\rho(n=k)=\exp(-\lambda k)\frac{(\lambda A)^{k}}{k!} \tag{6}$$

The mean value $E(\rho)$ and variance $D(\rho)$ of ρ are:

$$E(\rho)=\rho_0\left(1-\lambda\cdot A_0\right) \tag{7}$$

$$D(\rho)=\rho_0^2\cdot\frac{A_0^2}{A}\cdot\lambda \tag{8}$$

The mean value $E(\rho)$ and variance $D(\rho)$ of CT numbers corresponding to rock density distribution can be obtained by mathematical statistics of CT numbers. According to Formulas (7) and (8), the damage hole area A_0 and damage hole density λ can be calculated as follows:

$$A_0=\frac{D(\rho)\cdot A}{\rho_0\left[\rho_0-E(\rho)\right]} \tag{9}$$

$$\lambda=\frac{\rho_0\left[\rho_0-E(\rho)\right]^2}{D(\rho)\cdot A} \tag{10}$$

The damage formula based on cross-sectional area is as follows:

$$D_0=\frac{S-S_{\mathrm{ef}}}{S}=\frac{S_{\mathrm{d}}}{S}=\frac{\mathrm{n}\cdot\lambda\cdot A_0}{S} \tag{11}$$

where S is the cross-sectional area of the sample. S_{ef} is the effective area of the scanning section of the sample.S_{d} is the damage area of the sample. If the resolution of CT equipment is m_0 and the number of holes (cracks) in the resolution unit is $n=S/m_0$, the Formula (11) can be written as follows:

$$D_0=\frac{1}{m_0^2}\lambda A_0=\frac{1}{m_0^2}\left[1-\frac{E(\rho)}{\rho_0}\right] \tag{12}$$

The initial damage of basalt sample under high temperature heat treatment at 25℃ ~ 1000℃ can be obtained by Formula (12). The specific initial damage variable values are shown in Table 2. Based on the initial damage of 0.016 at 25 ℃, the stage characteristics of the initial damage growth ratio k are obvious after high temperature treatment

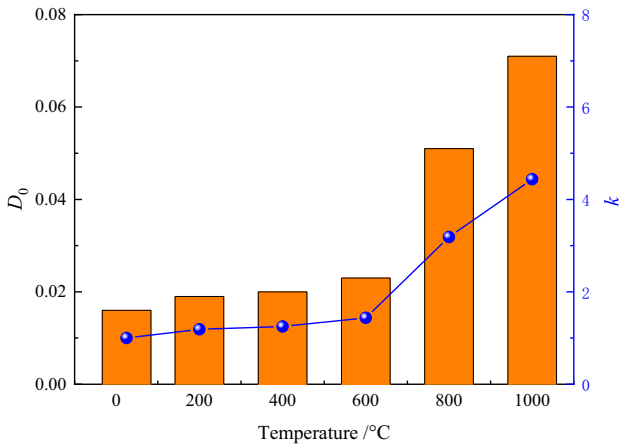

Fig. 11 Initial damage *D*0of basalt

at 200 ℃ ~ 1000 ℃. As a whole, there are two stages of low-speed deterioration and high-speed development (as shown in Fig. 11). When the heat treatment temperature is 200 ℃ ~ 600 ℃, the corresponding k value is within 1.118 ~ 1.437. When the temperature exceeds 800℃, the k value increases rapidly to 3.187 ~ 4.437.

4.2 Damage Evolution Characteristics of Basalt Under Triaxial Compression

4.2.1 Temporal and Spatial Distribution Characteristics of Microcracks

AE (acoustic emission) location technology based on Geiger algorithm (Zhao et al. 2008) is used to track the evolution process of fracture in rock samples under triaxial compression. As shown in Fig. 12, the magnitude of the AE source amplitude (unit: dB) is distinguished by the size and color of the sphere. The larger the AE amplitude, the larger the sphere size and the darker the color of the sphere, and vice versa. The evolution characteristics of basalt AE events are closely related to the macroscopic failure characteristics. With the increase of driving load, the AE signal gradually increases when the sample is destroyed, and the source amplitude is concentrated in 60 ~ 100 dB. When it is less than 40% of the peak stress, the AE events generated by acoustic emission are only scattered in the middle of the sample, indicating that the degradation begins from the middle and a nucleation zone is initially formed during compression. When the stress increases to 60% of the peak stress, the number of AE events increases sharply, the primary cracks continue to propagate, and the location of AE events corresponds to the main crack area of macroscopic failure. When the axial stress reaches 80% of the peak stress, the number of events expands rapidly to both sides based on the central fracture concentration zone. When the peak stress is reached, the number of AE events increases to the maximum, forming a fracture zone. The cracks eventually condense and penetrate, leading to rock failure. Under the action of high temperature heat treatment, the structure of basalt rock samples undergoes certain changes, which correspondingly affects the failure process. On the whole, with the increase of heat treatment temperature, the micro-fracture events of rock samples at the same stage increase sharply, especially when the load exceeds 40% of the peak stress, i.e., high temperature accelerates the failure process of basalt. Statistics of micro-fracture event information are shown in Table 3. Combined with the macroscopic failure diagram and sketch map of basalt, it can be found that when the temperature is lower than 400 °C, a number of oblique cracks with a certain angle to the direction of the principal stress are generated. A network of micro-crack areas is formed in the local area, accompanied by some shedding fragments. When the temperature exceeds 600 °C, the volume shows obvious lateral expansion, accompanied by strip surface peeling. The macroscopic cracks on the surface of the sample are mostly tensile cracks and basically consistent with the principal stress loading direction.

4.2.2 Evolution Characteristics of Damage Variable

Under external loads, the microcracks in rocks will continuously initiate, propagate, and aggregate, ultimately leading to rock instability and failure (Sarfarazi et al. 2021; Song et al. 2022). This progressive failure process of rock materials caused by the accumulation of micro-defects can be fed back by damage variable (Manthei 2005; Luo et al. 2020Yousefpour et al. 2022). Kachanov (1999) proposed the concept of continuity factor and damage stress, which is considered to have pioneered the discipline of damage mechanics. The damage variable is defined as follows.

$$D = \frac{A_d}{A_m} \tag{13}$$

where A_d is the cumulative projected area of all existing damages on the plane perpendicular to the stress direction, and A_m is the cross-sectional area at the initial undamaged state.

Assuming that the cumulative acoustic emission energy value for complete failure of the entire cross-sectional area *A*m is *E*0, the AE energy value for micro element failure per unit area is:

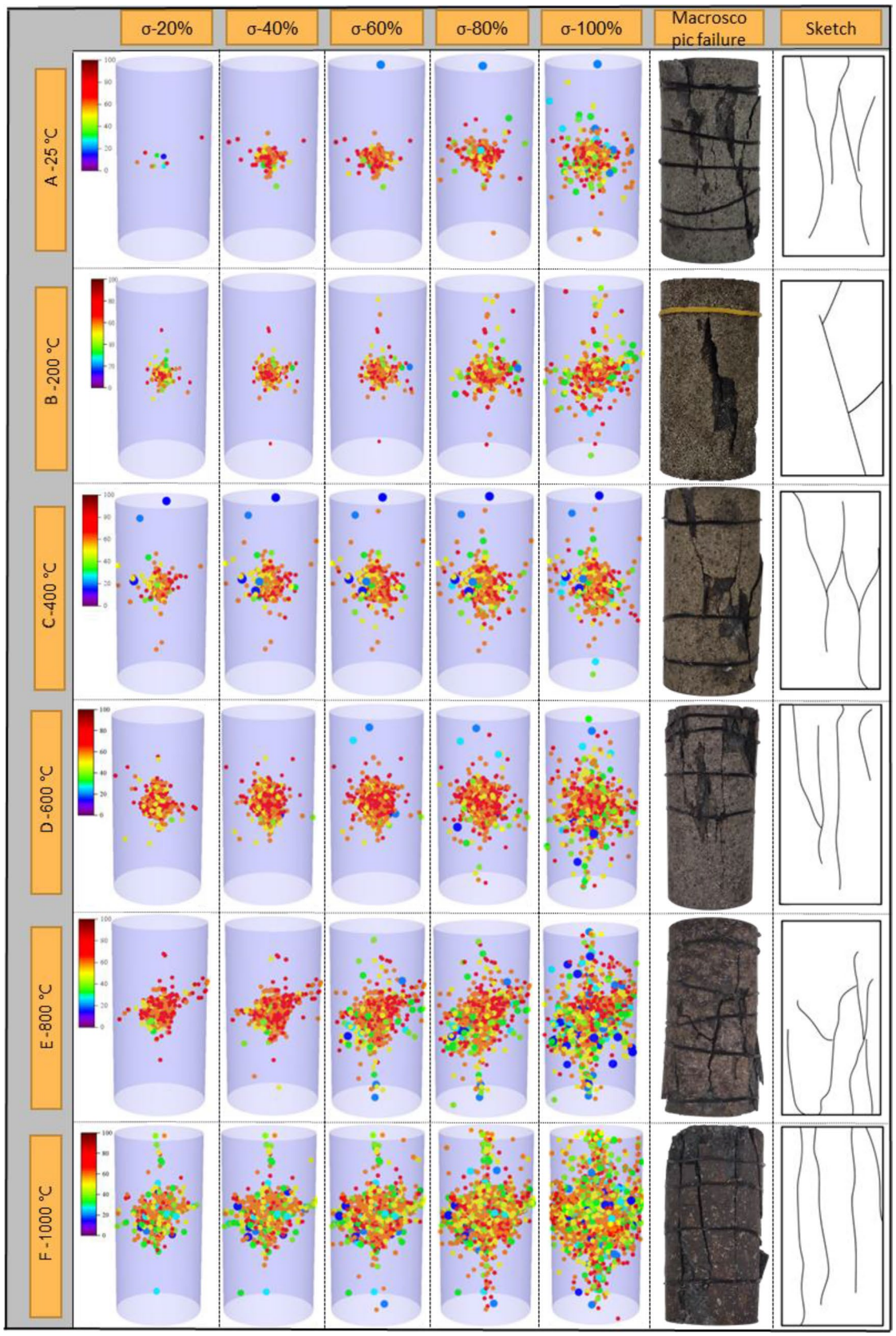

Fig. 12 Acoustic emission localization and macroscopic failure characteristics of basalt samples

Table 3 Number of AE events in each stage

No.	Temperature/℃	20% σ_{max}	40% σ_{max}	60% σ_{max}	80% σ_{max}	100% σ_{max}
A	25	383	764	1148	1531	1914
B	200	42	840	1260	1680	2100
C	400	741	1483	2223	2963	3706
D	600	1064	2129	3195	4260	5325
E	800	2974	5950	8926	11,903	14,880
F	1000	10,078	20,157	30,236	40,313	50,392

$$E_w = \frac{E_0}{A_m} \tag{14}$$

Therefore, when the cumulative damage area is Ad, the cumulative acoustic emission energy value is:

$$E_d = E_w A_d = \frac{E_0}{A_m} A_d \tag{15}$$

The rock damage variable represented by the acoustic emission energy value is:

$$D_1 = \frac{A_d}{A_m} = \frac{E_t}{E_0} \tag{16}$$

where, E_t is the energy released by acoustic emission of rock before the time t.

Overall, under the action of high temperature, the internal structure of rock undergoes mutual dislocation, which leads to the continuous increase of internal pores and cracks, resulting in initial damage (the first stage). The subsequent loading process exacerbates the damage (the second stage) and eventually leads to the failure of rock samples. Therefore, the total damage of basalt samples is the superposition of thermal damage caused by temperature change and structural progressive damage caused by load. By combining Formulas (12) and (16), the calculation formula of total damage D can be obtained.

$$D = D_0 + D_1 = \frac{1}{m_0^2}\left[1 - \frac{E(\rho)}{\rho_0}\right] + \frac{E_t}{E_0} \tag{17}$$

The evolution characteristics of D of basalt under thermal–mechanical action are obtained by Formula (17). As shown in Fig. 13, high temperature heat treatment has caused a certain degree of initial damage to the sample, so the damage D in the initial stage of loading is not zero, and the initial point gradually increases with the increase of heat treatment temperature. As the load increases, the change of rock damage is not obvious. At this time, the stress–strain curve is in the stages of pore fracture compaction and linear elasticity. The increase of external load has no significant effect on the overall structure of rock. When the driving load further increases, the rock damage variable shows a small increase, and the stress–strain curve synchronously shows a nonlinear growth characteristic, i.e., the rock sample structure undergoes irreversible deterioration. When the driving load tends to the peak point, the damage variable increases sharply and reaches 1, i.e., the rock material completely loses its bearing capacity. In addition, it can be observed that when the temperature is less than 400 ℃, the transition time of the damage variable D from the initial stable stage (small magnitude) to 1 is extremely short, showing a remarkable sudden feature, and the failure precursor is not obvious, which is consistent with the brittle characteristics of basalt samples in Sect. 3.1. When the temperature exceeds 400 ℃, continuous damage will occur in the rock before the peak, and the damage variable D will increase slightly between the stable stage and the drastic stage, and the characteristics of this stage will become more and more obvious as the temperature gradually approaches 1000 ℃.

Furthermore, the rock damage variables of each stage are statistically analyzed. As shown in Fig. 14, the D of basalt shows an upward trend with the increase of stress. At the initial stage of loading, the damage variable is mainly the initial damage D_0 after high temperature treatment. The D_0 below 600 ℃ is small, which is consistent with the law shown by CT scanning pore diagram. When the heating temperature reaches 800 °C and 1000 °C, the pores and cracks in the sample are more developed, so the initial damage is larger. When the stress of the sample exceeds 60% of the ultimate stress, new cracks are generated in the rock under compression, corresponding to the unstable fracture development stage in Sect. 3.1. The material shows certain yield characteristics correspondingly. Especially when the temperatures are 800℃ and 1000℃, the damage degree increases significantly. This evolution characteristic is consistent with the development of stress–strain and micro-fracture events, indicating the rationality and feasibility of the damage model proposed in this study.

4.3 Composition Analysis of Basalt After Heat Treatment

Rock is a heterogeneous material composed of different mineral components. To analyze the influence of high temperature treatment on the internal mineral components of

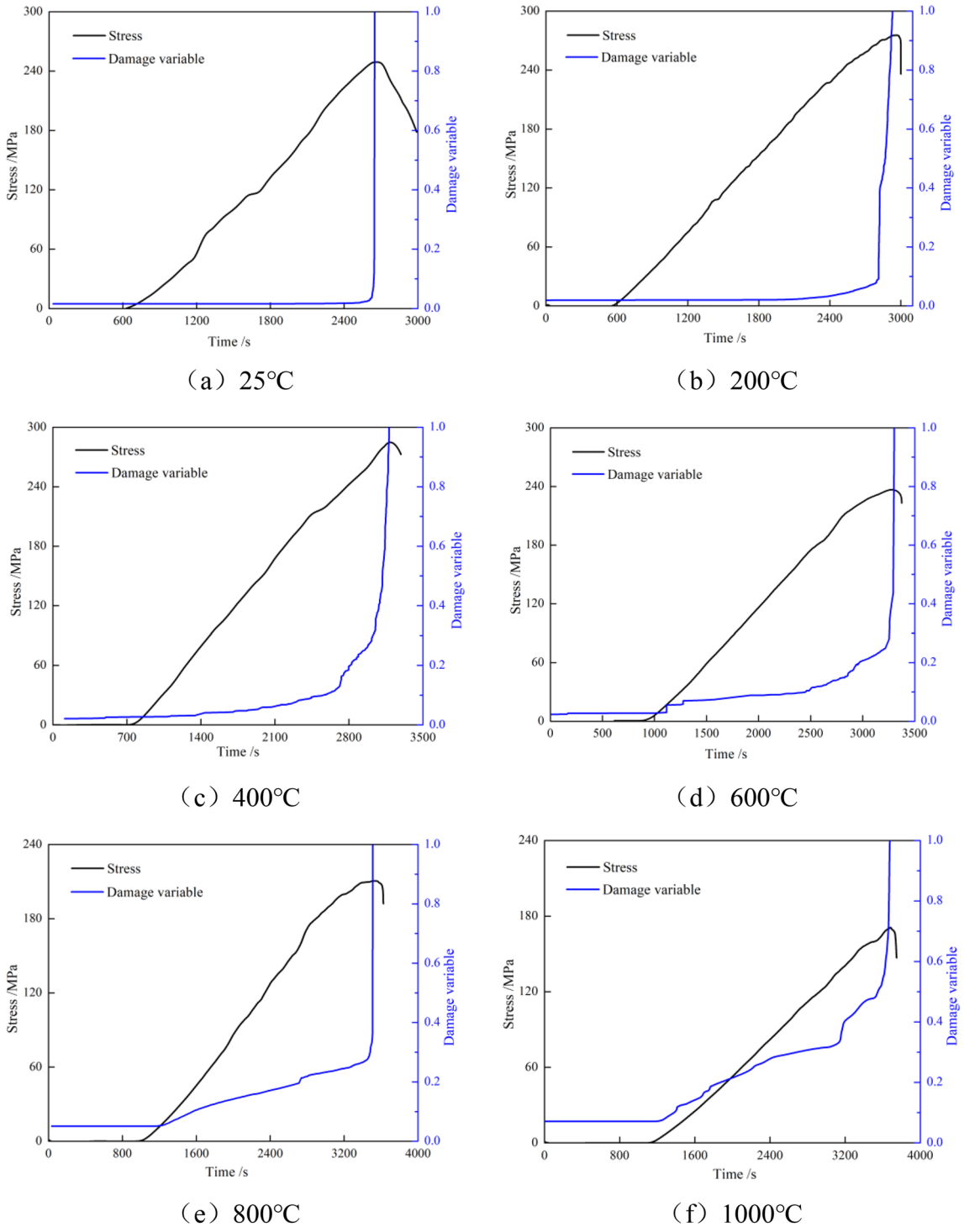

Fig. 13 Damage evolution curve of basalt

the sample, XRD is used to quantitatively analyze the rock sample exposed to high temperature treatments. Figure 15 shows the XRD analysis of basalt after different high temperature treatments. The larger the diffraction peak is, the higher the content of mineral components in the reaction is. The diffraction patterns of basalt samples after different temperature treatments are similar, i.e., the main mineral types (andesine, anorthite, enstatite) have not changed. In view of the peak intensity, the relative content of main

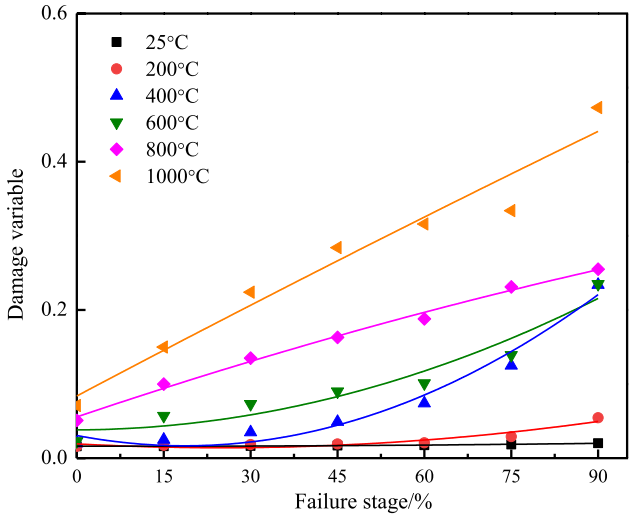

Fig. 14 Basalt damage variables in each stage

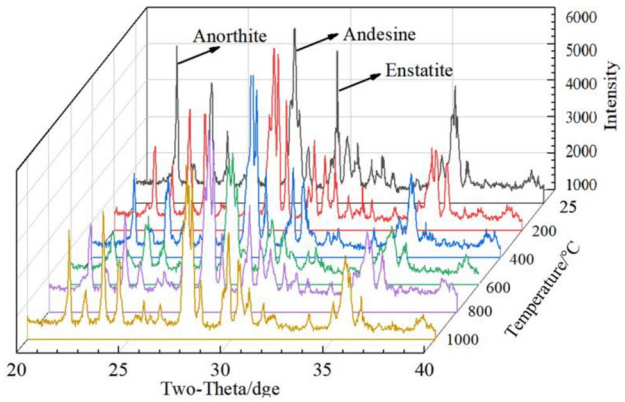

Fig. 15 XRD analysis of basalt exposed to different temperature treatments

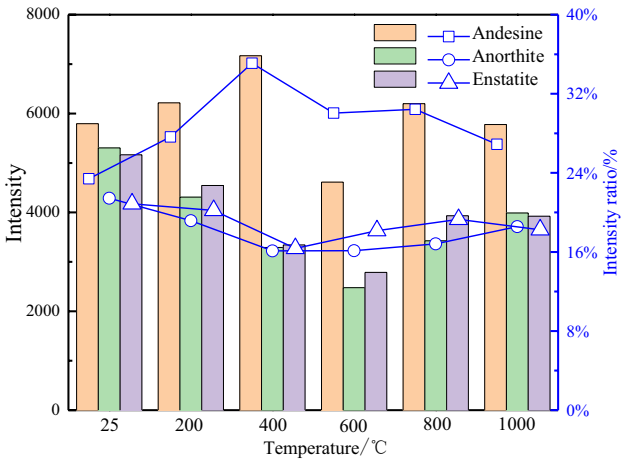

Fig. 16 Relative intensity of diffraction peaks of main components of basalt

minerals has changed, while the corresponding changes of other components are relatively small.

The composition change of rock under high temperature is one of the fundamental reasons that affect the mechanical properties of basalt (Orabi 2022; Soesoo et al. 2021). Figure 16 shows the relative intensity change and intensity ratio curves of the diffraction peaks of the main components of basalt exposed to high temperature treatment. As a heat-sensitive mineral, andesine has the characteristics of high temperature resistance, corrosion resistance, strong brittleness and high strength (Ghadami and Nazarinia 2022). Anorthite has the characteristics of low thermal expansion coefficient, small bulk density, high strength and low sintering temperature (Pei et al. 2021). Enstatite is a wave-absorbing sensitive mineral, which belongs to silicate rock-forming mineral and has the characteristics of high temperature resistance (Lu et al. 2020). When the heat treatment temperature increases from 25 to 400 ℃, the diffraction peak intensity of andesine in basalt gradually increases, and the intensity ratio increases from 23.41 to 35.09%. Anorthite and enstatite is relatively consistent, and the intensity ratios decrease from the initial 21.43% and 20.87% to 16.11% and 16.35%. As the heat treatment temperature continues to increase, the diffraction peak intensity of andesine deteriorates. When the temperature is heated to 1000 ℃, the diffraction peak intensity ratio decreases to 26.89%. The intensity ratios of anorthite and enstatite have upward trends correspondingly, reaching 18.56% and 18.25% (see Table 4 for details). The composition change of basalt under the action of high temperature will have a certain influence on the mechanical properties of rock.

4.4 Comparison of Thermal Damage Laws of Common Rocks

Granite, sandstone, marble, and basalt are common types of rocks in rock engineering. The mechanical properties and failure mechanisms of these rocks have always been of interest to scholars (Ercenk et al. 2018; Zhai et al. 2020; Sokairge et al. 2022; Aidaraliev et al. 2021; Silva et al. 2021). To understand the thermal damage laws of different types of rocks, Fig. 17 summarizes the test results of some scholars (Du et al. 2004; Wu et al. 2007, 2012; Zhang et al. 2009, 2011; Chen et al. 2011; Chen and Yang 2014; Liu and Xu 2015; Su et al. 2017; Rathnaweera et al. 2018; Qin et al. 2020; Liang et al. 2021; Qi et al. 2021; Yang et al. 2022). It should be noted that the current research on the thermal damage laws of rock mechanics is almost all based on the uniaxial compression performance of rocks. However, by comparing these data, the differences in the thermal damage laws of these four types of rocks can still be observed.

Table 4 Proportion of basalt composition

Component	Component ratio/%					
	25℃	200℃	400℃	600℃	800℃	1000℃
Andesine	23.41	27.63	35.09	30.04	30.43	26.89
Anorthite	21.43	19.16	16.11	16.14	16.81	18.56
Enstatite	20.87	20.20	16.35	18.15	19.30	18.26
Others	34.29	33.01	32.45	35.67	33.46	36.29

Combining Figs. 7 and 17, although the results of tests in different studies vary greatly, both the compressive strength and elastic modulus characteristics are affected by the heat treatment temperature. The differences in these test results may be related to the heterogeneity caused by natural defects inside the rock. In addition, some experimental data in certain studies show certain fluctuations, but the compressive strength and elastic modulus of the four types of rocks all show a decreasing trend with increasing temperature, and there is a temperature threshold for each of them. Specifically, as the heat treatment temperature increases, these two mechanical performance indicators slowly decrease or exhibit slight fluctuations. When the heat treatment temperature exceeds a certain temperature threshold, these two mechanical performance indicators will drop sharply. The comparison between Figs. 7 and 17 further reveals that there are also differences in the temperature thresholds among these four types of rocks. Basalt has the highest temperature threshold, followed by granite and sandstone, with little difference between the two, and finally marble. Rocks are aggregates composed of various minerals, and the fundamental causes of deterioration in their mechanical properties may be related to changes in the mineral composition and crystal phase transformation. The differences in the thermal damage laws of these four types of rocks may be related to differences in their crystal structures, mineral compositions, and their contents.

5 Conclusions

To explore the mechanical properties and damage characteristics of basalt under high temperature and high pressure, triaxial compression tests are conducted on thermal damage samples, and the evolution process from progressive damage to macroscopic failure of basalt is tracked and quantified using CT image reconstruction and acoustic emission technology. The main conclusions are as follows.

(1) Under high temperature and high pressure conditions, the peak strength and elastic modulus of basalt show a trend of first increasing and then decreasing with the increase of temperature. The peak strength and elastic modulus reach the maximum at 400 °C. Compared with the room temperature state, the maximum increases in peak strength and elastic modulus are 15.85% and 9.37%, respectively. When the temperature exceeds 400 ℃, the peak strength and elastic modulus of the rock deteriorate significantly, with degradation of 30.44% and 53.72% at 1000 ℃, respectively. In addition, due to the increase of temperature, the failure mode of basalt transforms from brittleness to plasticity, and the post-peak stress gradually presents plastic flow characteristics.

(2) The structural characteristics of rock thermal damage can be quantitatively reflected by CT three-dimensional image reconstruction. With the gradual change of temperature environment from 25 ℃, 600 ℃ to 1000 ℃, the porosity of rock is 6.86%, 7.56% and 18.02%, respectively, and the D_0 is 0.016, 0.023 and 0.071, respectively. The structural deterioration trend is characterized by obvious stage characteristics from low-speed development to rapid growth.

(3) The failure of heat treatment basalt mainly begins in the middle of the sample and continues to expand. As the temperature increases, the rock sample gradually changes from tensile-shear composite failure to tensile splitting failure. When the temperature is less than 400 ℃, the process from initial micro damage to failure of the rock exhibits a significant suddenness. When the temperature exceeds 400 ℃, continuous damage will occur inside the rock before the peak stress. There is a small growth transition stage before the D undergoes a drastic change, and this characteristic becomes more obvious with the increasing temperature.

(4) The main mineral types of basalt hardly change with the increasing temperature, but the temperature has a certain influence on the proportion of some components. As the temperature increases, the proportion of andesine shows an upward convex evolution of first increasing and then decreasing, accounting for 23.41%, 35.09% and 26.89% at 25℃, 400℃ and 1000℃, respectively. The evolution characteristics of anorthite and enstatite are relatively consistent, showing the change characteristics of first decreasing and then increasing. The composition

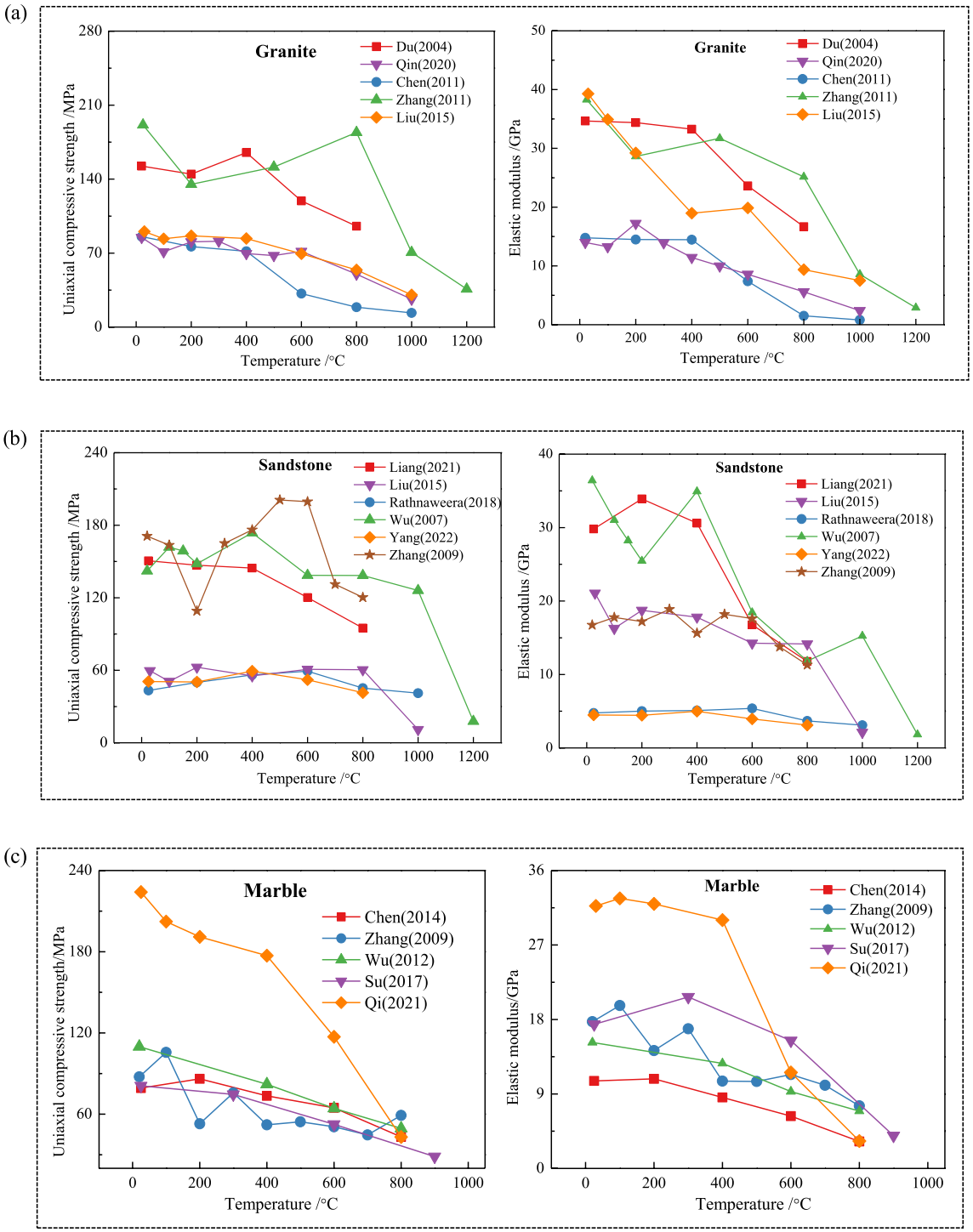

Fig. 17 Comparison of the thermal damage to different rocks

change of rock under high temperature will directly affect the mechanical properties of rock.

(5) Within the temperature threshold, the expansion of mineral particles and confining pressure constraint will lead to the gradual closure of primary cracks and increase the compactness of rocks, which is also the main reason for the improvement of rock mechanical properties. When the heat treatment temperature exceeds the threshold, the

structural deterioration caused by heat treatment will gradually become prominent, and the defects generated inside the sample play a leading role in the mechanical properties of the rock.

Acknowledgements The project was supported by the National Natural Science Foundation of China (No. 42002275), Natural Science Foundation of Zhejiang province (No. LQ21D020001), China Postdoctoral Science Foundation (No. 2021M692319; 2023M732689), Shaoxing Science and Technology Plan Project(No.2022A13003).

Author Contributions GW: writing—review & editing, data curation, investigation, visualization. LS: conceptualization, methodology, formal analysis, funding acquisition. XL: formal analysis, data curation, conceptualization, funding acquisition. XM: formal analysis, data curation, conceptualization. JQ: review and editing, data curation. HC: data curation, funding acquisition. LW: formal analysis, funding acquisition.

Funding National Natural Science Foundation of China, 42002275,Leibo SONG, Natural Science Foundation of Zhejiang Province, LQ21D020001, Leibo SONG, China Postdoctoral Science Foundation,2021M692319,Leibo SONG, 2023M732689,Gang Wang, Shaoxing Science and Technology Plan Project, 2022A13003, Gang Wang.

Data Availability All data generated or analyzed during this study are included in this published article.

References

Aidaraliev Z, Rysbaeva I, Atyrova R, Abdykalykov A, Kyzy BB, Zholdoshova C, Abdullaeva Z (2021) Suitability of Suluu-Terek basalt deposits for stone casting. J Miner Mater Charact Eng 10(1):1–14

Braun P, Ghabezloo S, Delage P, Sulem J, Conil N (2021) Thermo-poro-elastic behaviour of a transversely isotropic shale: thermal expansion and pressurization. Rock Mech Rock Eng 54:359–375

Brown ET (1981) Rock characterization, testing & monitoring: ISRM suggested methods. Pergamon Press, Oxford

Chen GF, Yang SQ (2014) Study on failure mechanical behavior of marble after high temperature. J Eng Mech 31(8):189–196

Chen YL, Wei S, Zhou YC (2011) Experimental study on mechanical properties of granite after high temperature. Chin Q Mech 71:3349–3354

DasGupta S, Slobodyan O, Smith T, Binder A, Flicker J, Kaplar R, Atcitty S (2022) Identification of the defect dominating high temperature reverse leakage current in vertical GaN power diodes through deep level transient spectroscopy. Appl Phys Lett 120(5):053502

Du S, Liu H, Zhi H, Chen H (2004) Testing study on mechanical properties of post-high-temperature granite. Chin J Rock Mech Eng 23:2359–2364

Ercenk E, Guven B, Yilmaz S (2018) Crystallization kinetics of machinable glass ceramics produced from volcanic basalt rock. J Non-Cryst Solids 498:262–271

Garcia-Ramonda L, Pelà L, Roca P, Camata G (2022) Cyclic shear-compression testing of brick masonry walls repaired and retrofitted with basalt textile reinforced mortar. Compos Struct 283:115068

Gautam PK, Verma AK, Sharma P, Singh TN (2018) Evolution of thermal damage threshold of Jalore granite. Rock Mech Rock Eng 51:2949–2956

Ghadami GR, Nazarinia A (2022) Adakite signatures in granitoids northwest of Shahr-e-Babak, Kerman, Iran: constraints from geochemistry. J Mineral Geochem 197(3):263–283

Ghamgosar M, Bahaaddini M, Erarslan N, Williams DJ (2021) A new experimental approach to quantify microfractures in the fracture process zone (FPZ) under various loading conditions. Eng Geol 283:106024

Huang YH, Yang SQ, Bu YS (2020) Effect of thermal shock on the strength and fracture behavior of pre-flawed granite specimens under uniaxial compression. Theoret Appl Fract Mech 10(6):102474

Kachanov LM (1999) Rupture time under creep conditions. Int J Fract 97(1):11–18

Kuncham E, Sen S, Kumar P, Pathak H (2022) An online model-based fatigue life prediction approach using extended Kalman filter. Theoret Appl Fract Mech 117:103143

Li LP, Jia C, Sun ZZ (2021) Research status and development trend of major engineering disaster prevention and control technology in deep underground. J Central South Univ (Sci0 Technol) 52(08):2539–2556

Liang S, Fang SZ, Wei GH, Zhu XL, Li WY, Ma JQ (2021) Experiments on mechanical properties of siliceous sandstone after high temperature. J Zhengzhou Univ 42(3):87–92

Liu S, Xu JY (2015) An experimental study on the physico-mechanical properties of two post-high-temperature rocks. Eng Geol 18(5):63–70

Liu Z, Wang C, Zhou H, Shen W, Shao J (2021) A true triaxial time-dependent test system with two rigid and one flexible loading frame for rock under real-time high temperature and high pressure and its application. Chin J Geotech Eng 40(12):2477–2486

Liu L, Li R, Qin H, Liu Y (2022) Dynamic mechanical properties and microscopic damage characteristics of deep skarn after high-temperature treatment. Chin J Geotech Eng 44(6):1166–1174

Liu X, Wang G, Song L, Han G, Chen W, Chen H (2023) A new rockburst criterion of stress–strength ratio considering stress distribution of surrounding rock. Bull Eng Geol Env 82(1):29

Lu G, Zhou J, Bing Z, Pan D, Tong T (2020) Damage, deformation and energy characteristics of basalt after microwave irradiation subjected to cyclic loading. Tunnel Constr 40(11):1578

Luo Y, Wang G, Li X, Liu T, Mandal AK, Xu M, Xu K (2020) Analysis of energy dissipation and crack evolution law of sandstone under impact load. Int J Rock Mech Min Sci 132:104359

Ma X, Ma D, Hu D, Zhou H, Chen S, Yu Z, Tan X (2019) A real-time high-temperature true triaxial test system and its application. Chin J Rock Mech Eng 38(08):1605–1614

Manthei G (2005) Characterization of acoustic emission sources in a rock salt specimen under triaxial compression. Bull Seismol Soc Am 95(5):1674–1700

Miao S, Pan PZ, Zhao X, Shao C, Yu P (2021) Experimental study on damage and fracture characteristics of Beishan granite subjected to high-temperature treatment with DIC and AE techniques. Rock Mech Rock Eng 54:721–743

Niu Y, Hu Y, Wang J (2023) Cracking characteristics and damage assessment of filled rocks using acoustic emission technology. Int J Geomech 23(4):04023013

Orabi EA (2022) The environment deterioration impact on the granite rock art relief of seti I in aswan, Egypt. J Mater Sci Chem Eng 10(10):20–39

Pan X, Huang J, Gan Z, Hua W, Dong S (2021) Investigation on mixed-mode II-III fracture of the sandstone by using eccentric cracked disk. Theoret Appl Fract Mech 115:103077

Pei D, Li Y, Hua S, Li S, Jiang F, Yao J (2021) In situ XRD study on function mechanism of pyroxene and anorthite in Si-Ca ceramics from ferronickel slag. Mater Lett 305:130839

Qi HY, Liu L, Meng X (2021) Study on the static and dynamic characteristics of marble at different temperature. Ind Miner Process 50(6):25–30

Qin Y, Tian H, Xu NX, Chen Y (2020) Physical and mechanical properties of granite after high-temperature treatment. Rock Mech Rock Eng 53(1):305–322

Rathnaweera TD, Ranjith PG, Gu X, Perera MSA, Kumari WGP, Haque A, Li JC (2018) Experimental investigation of thermo-mechanical behaviour of clay-rich sandstone at extreme temperatures followed by cooling treatments. Int J Rock Mech Min Sci 10(7):208–223

Sangsefidi M, Akbardoost J, Zhaleh AR (2021) Assessment of mode I fracture of rock-type sharp V-notched samples considering the size effect. Theoret Appl Fract Mech 116:103136

Sarfarazi V, Abharian S, Ghorbani A (2021) Physical test and PFC modelling of rock pillar failure containing two neighboring joints and one hole. Smart Struct Syst 27:123–137

Shi X, Jing H, Yin Q, Zhao Z, Han G, Gao Y (2020) Investigation on physical and mechanical properties of bedded sandstone after high-temperature exposure. Bull Eng Geol Env 79:2591–2606

Silva B, Calegari MR, Pinheiro MR, Fujita RH (2021) Lithostructural and tectonic determinants in the geomorphic evolution of the Basalt Plateau-Southern Brazil. J S Am Earth Sci 110:103351

Soesoo A, Nirgi S, Urtson K, Voolma M (2021) Geochemistry, mineral chemistry and pressure-temperature conditions of the Jõhvi magnetite quartzites and magnetite-rich gneisses, NE Estonia. Estonian J Earth Sci 70(2):71–79

Sokairge H, Elgabbas F, Elshafie H (2022) Structural behavior of RC beams strengthened with prestressed near surface mounted technique using basalt FRP bars. Eng Struct 250:113489

Song L, Wang G, Wang X, Huang M, Xu K, Han G, Liu G (2022) The influence of joint inclination and opening width on fracture characteristics of granite under triaxial compression. Int J Geomech 22(5):04022031

Song L, Zhang D, Wang G, Du S, Hu G, Han G, Wang X, Liu X (2023) Evaluation method of local failure characteristics for joint based on white light scanning technology. Nat Hazards 116(1):97–110

Su H, Jing H, Yin Q, Yu L, Wang Y, Wu X (2017) Strength and deformation behaviors of veined marble specimens after vacuum heat treatment under conventional triaxial compression. Acta Mech Sin 33(5):886–898

Vaneghi RG, Saberhosseini SE, Dyskin AV, Thoeni K, Sharifzadeh M, Sarmadivaleh M (2021) Sources of variability in laboratory rock test results. J Rock Mech Geotech Eng 13(5):985–1001

Wang T, Wang L, Xue F, Xue M (2021a) Identification of crack development in granite under triaxial compression based on the acoustic emission signal. Int J Distrib Sens Netw 17(1):1550

Wang Y, Hu S, He Z (2021b) Mechanical and fracture properties of geopolymer concrete with basalt fiber using digital image correlation. Theoret Appl Fract Mech 112:102909

Wang G, Luo Y, Gong H, Liu T, Li X, Song L (2023a) Investigations on the macro-meso mechanical properties and energy dissipation mechanism of granite shear fracture under dynamic disturbance. Int J Numer Anal Meth Geomech 2023:1–21

Wang G, Liu X, Chang Y, Song L, Zhou C, Wang Z (2023b) Analysis on rockburst failure energy evolution of model specimen under stress gradient. Rock Mech Rock Eng 2023:1–14

Wu G, Xing A, Zhang L (2007) Mechanical characteristics of sandstone after high temperatures. Chin J Rock Mech Eng 26(10):2110–2116

Wu G, Wang D, Zhai S, Li Y, Chen J (2012) Test research on mechanical properties of marble under high temperature. Chin J Rock Mech Eng 31(6):1237–1244

Xu X, Gao F, Zhang Z, Chen L (2015) Experimental study of the effect of loading rates on mechanical properties of granite at real-time high temperature. Rock and Soil Mech 36(08):2184–2192

Yang K, Fang JJ, Tang JZ, Liu WJ (2022) Uniaxial compression tests on red sandstone specimens after different high-temperature processing and cooling time. Bull Eng Geol Env 81(9):10–16

Yin T, Wang C, Wu Y, Wu B (2021) A waveform modification method for testing dynamic properties of rock under high temperature. J Rock Mech Geotech Eng 13(4):833–844

Zhai S, Su G, Yin S, Zhao B, Yan L (2020) Rockburst characteristics of several hard brittle rocks: a true triaxial experimental study. J Rock Mech Geotech Eng 12(2):279–296

Zhang LY, Mao XB, Lu AH (2009) Experimental study on the mechanical properties of rocks at high temperature. Sci China Ser E-Tech Sci 52(3):641–646

Zhang ZZ, Gao F, Xu XL (2011) Experimental study of temperature effect of mechanical properties of granite. Rock Soil Mech 32(8):2346–2352

Zhao XD, Liu JP, Li YH, Tian J, Zhu WC (2008) Experimental verification of rock locating technique with acoustic emission. Chin J Geotech Eng 30(10):1472–1476